Multicenter Reproducibility of ^{18}F-Fluciclatide PET Imaging in Subjects with Solid Tumors

Rohini Sharma[1], Kumar G. Kallur[2], Jin S. Ryu[3], Ramanathapuram V. Parameswaran[4], Henrik Lindman[5], Norbert Avril[6], Fergus V. Gleeson[7], Jong D. Lee[8], Kyung-Han Lee[9], Michael J. O'Doherty[10], Ashley M. Groves[11], Matthew P. Miller[12], Edward J. Somer[12], Charles R. Coombes[13], and Eric O. Aboagye[13]

[1]Department of Experimental Medicine, Faculty of Medicine, Imperial College London, Hammersmith Hospital, London, United Kingdom; [2]PETCT and Cyclotron Department, HCG, Bangalore, India; [3]Department of Nuclear Medicine, Asan Medical Center, Seoul, South Korea; [4]Department of Nuclear Medicine and PET-CT Division, Manipal Hospital, Bangalore, India; [5]Uppsala University Hospital, Department of Oncology, Uppsala, Sweden; [6]Department of Nuclear Medicine, Barts Health, Queen Mary University of London, London, United Kingdom; [7]Department of Radiology, Churchill Hospital, Oxford Radcliffe Hospitals Trust, Oxford, United Kingdom; [8]Department of Nuclear Medicine, Yonsei University Health System, Seoul, Korea; [9]Department of Nuclear Medicine, Samsung Medical Center, Seoul, Korea; [10]PET Imaging Centre, Division of Imaging Sciences and Biomedical Engineering, King's College London, London, United Kingdom; [11]Institute of Nuclear Medicine, University College London, London, United Kingdom; [12]GE Healthcare Life Sciences, Imaging R&D, Amersham, United Kingdom; and [13]Department of Surgery and Cancer, Faculty of Medicine, Imperial College London, Hammersmith Hospital, London, United Kingdom

Integrins are upregulated on both tumor cells and associated vasculature, where they play an important role in angiogenesis and metastasis. Fluciclatide is an arginine-glycine-aspartic acid peptide with high affinity for $\alpha_v\beta_3/\alpha_v\beta_5$ integrin, which can be radiolabeled for PET imaging of angiogenesis. Thus, ^{18}F-fluciclatide is a potential biomarker of therapeutic response to antiangiogenic inhibitors. The aim of this study was to evaluate the reproducibility of ^{18}F-fluciclatide in multiple solid-tumor types. **Methods:** Thirty-nine patients underwent PET/CT scanning at 40, 65, and 90 min after injection of ^{18}F-fluciclatide (maximum, 370 MBq) on 2 separate days (2–9 d apart). Patients did not receive any therapy between PET/CT scans. ^{18}F-fluciclatide images were reported and quantitative measures of uptake were extracted using the PERCIST methodology. Intrasubject reproducibility of PET uptake in all measurable lesions was evaluated by calculating relative differences in SUV between PET scans for each lesion during the 2 imaging sessions. **Results:** Thirty-nine measurable lesions were detected in 26 patients. Lesion uptake correlated strongly across imaging sessions ($r = 0.92$, $P < 0.05$, at 40 min; $r = 0.94$, $P < 0.05$, at 65 min; $r = 0.94$, $P < 0.05$, at 90 min) with a mean relative difference and SD of the relative difference of 0.006 ± 0.18 at 40 min, 0.003 ± 0.19 at 65 min, and 0.025 ± 0.20 at 90 min. This reflects 95% limits of repeatability of 35%–39% for the difference between the 2 SUV measurements or a variability of 18%–20% in agreement from that observed in well-calibrated multicenter ^{18}F-FDG studies. **Conclusion:** The test–retest reproducibility of ^{18}F-fluciclatide across multiple tumor types has been measured and shown to be acceptable. This is an important step in the development of this in vivo biomarker to identify and quantify response to antiangiogenic therapy in cancer patients.

Tumor angiogenesis, the formation of tumor-associated vasculature, is an essential event in tumor growth and metastasis and has been the focus of therapeutic target development for decades (*1*). Several antiangiogenic therapies are routinely used for the management of solid tumors, including bevacizumab for management of colorectal and ovarian cancer (*2–5*), sunitinib and pazopanib for metastatic renal cell cancer (*6,7*), and sorafenib for hepatocellular cancer (*8*). Using conventional imaging assessment, these agents predominantly result in a cytostatic response, with changes in tumor size taking months to evolve. Furthermore, these agents are associated with significant toxicity profiles, including hypertension, gastrointestinal perforation, and hemorrhage. Therefore, there is a real need for a validated biomarker of therapeutic response to differentiate those patients benefiting from these targeted agents and those being exposed to potential life-threatening toxicities without clinical effect.

As new vessels form, integrins, a family of cell adhesion molecules, facilitate the interaction between tumor vasculature and the extracellular matrix (*9,10*). $\alpha_v\beta_{3/5}$ integrins are of particular interest as these are expressed at low levels on mature vessels and nonneoplastic epithelium but are highly expressed on activated tumor-related endothelial cells, as well as cancers such as breast and lung cancer, melanoma, and osteosarcoma (*9,11*). $\alpha_v\beta_{3/5}$ integrins interact with components of the extracellular matrix such as fibronectin, laminin, and collagen via the tripeptide sequence arginine-glycine-aspartic acid (RGD) (*12*). Peptide ligands have high affinity for the RGD sequence, and several radiolabeled probes, have been developed to image integrin expression either with PET or with SPECT (*13–17*). Given the pivotal role that these integrins hold in tumor angiogenesis and cancer progression, the

ability to visualize and quantify $\alpha_v\beta_3/\alpha_v\beta_5$ integrin presents an opportunity to develop a response biomarker.

[18]F-fluciclatide is a cyclic tripeptide that contains the RGD sequence and binds with high affinity to integrins $\alpha_v\beta_3$ and $\alpha_v\beta_5$, both of which are upregulated in tumor-associated vasculature (18). ^{18}F-fluciclatide is currently being developed as a radiotracer for the imaging of angiogenesis in tumors and consequently as a biomarker of response to antiangiogenic therapies (14,19).

Imaging biomarkers used in any prognostic or treatment response studies should exhibit a high degree of reproducibility such that a significant change in imaging parameters between 2 studies can be considered relevant and not attributable to noise variance. Quantification of intrinsic variability in the absence of treatment is important to provide a robust objective response criterion such as PERCIST for ^{18}F-FDG PET (20). Therefore, test–retest measurements are an essential step in the clinical development of any new PET tracers. The Quantitative Imaging Biomarker Alliance has listed repeatability metrics commonly found in the literature (21). Although mean absolute percentage difference in SUV appears to be the most common measure assessed, mean relative difference and the SD of the relative differences provides information on both systematic and random error. Additionally, this approach allows calculation of a measure of reproducibility reflecting the 95% confidence limits for identification of a true difference between the 2 measurements, such that measured changes in tumor uptake that fall outside this 95% coefficient of repeatability can be attributed to biologic response (22). An appreciation of test variability is also a requirement for correct powering of single and multicenter controlled trials. The sample size depends on both the effect size (expected treatment group difference) and the response variance. Consequently, studies using a test with high test–retest variability will require a larger subject cohort than one with lower variability to demonstrate the same effect (23). Therefore, the primary objective of this study was to assess the test–retest reproducibility of ^{18}F-fluciclatide uptake in solid tumors within a multicenter setting.

MATERIALS AND METHODS

Patients

Ethical approval was obtained before the study commenced, and all procedures were in accordance with the ethical standards of the responsible committee on human experimentation and with the Helsinki Declaration of 1975, as revised in 2008. Thirty-nine patients were enrolled into this multicenter study. All had at least one solid primary or metastatic tumor 2.0 cm or larger in diameter, including but not limited to non–small cell lung cancer, renal cell cancer, glioblastoma, melanoma, sarcoma, head and neck cancer, and breast cancer. Only patients not undergoing curative treatment and who had undergone routine clinical imaging within 8 wk of study entry were eligible. Patients who had undergone biopsy, radiotherapy, surgery, or any other treatment within 4 wk before the first imaging session (within 2 wk of chemotherapy) or were scheduled to undergo such procedures between the first and second ^{18}F-fluciclatide PET sessions were ineligible. Patients who were pregnant, lactating, or not practicing adequate contraception were also excluded. All subjects were required to give signed and dated informed consent to take part in the study.

Study Design

The aim of the study was to determine the reproducibility of serial ^{18}F-fluciclatide PET scans and to define objective ^{18}F-fluciclatide response parameters. To this end, patients underwent 2 ^{18}F-fluciclatide sessions within 10 d of each other before commencement of therapy.

PET Imaging

Radiolabeled active ^{18}F-fluciclatide was formulated in phosphate-buffered saline containing up to 7% w/v ethanol and a 2 mg/mL concentration of sodium p-aminobenzoate as a ready-to-use sterile solution (18) at a qualified, good-manufacturing-practice–validated facility. Before administration, the suitability of each preparation was assessed by radioactivity, high-performance liquid chromatography, and pH measurement, according to the approved standard operating procedures of the facility. A maximum of 20 μg of fluciclatide peptide was administered in a single intravenous bolus at each ^{18}F-fluciclatide imaging session. The pH of the solution was 6–8. The radiochemical purity of ^{18}F-fluciclatide injection was not less than 90% during the shelf life of the product. The maximum dose for radioactivity was 370 MBq for each scan. ^{18}F-fluciclatide was administered as a bolus dose over 10 s, followed by a 10-mL saline flush. Thirty-five minutes after injection, a short CT scan was performed followed by a low-dose, whole-body CT scan for attenuation correction and anatomic localization. Three-dimensional whole-body PET acquisitions were obtained at 3 time points with nominal start times at 40, 65, and 90 min after injection. Emission data were reconstructed using iterative ordered-subset expectation maximization and filtered backprojection. Reconstruction was performed with 8 iterations and 21 subsets; the voxel size ranged between 1.277 and 1.788 mm^3 and was consistent across centers.

Site Qualification and Quality Control

All subjects were imaged on a dedicated, full-ring PET/CT scanner (Discovery models STE x4, ST x2, VCT, Rx, 690, and 600 [GE Healthcare]; Gemini TF [Philips]). Participating sites were required to submit recently acquired test data to the sponsor for review before the commencement of scanning. Using these data, image reconstruction parameters were adjusted when necessary to minimize intersite variability to allow the pooling of data. ^{18}F-fluciclatide image quality and protocol adherence was monitored throughout the study. Standard-of-care images did not undergo formal quality control.

Image Acquisition and Analysis

Uptake Characteristics. Tumor uptake characteristics were determined from the 40-min acquisition scan of the first PET session. PERCIST-type analysis was undertaken by a single interpreter who was masked to scan timing and clinical history (20). For each lesion, volume of interest was used to determine tracer uptake, denoted as SUV$_{peak}$, and was normalized to body weight. When a suitable region of tissue could be identified, a 3-cm-diameter region of interest, as described by the PERCIST methodology, was placed over healthy liver to determine the intersubject variability of liver SUV$_{mean}$ normalized to body weight (SUV$_{liver}$) across the 3 time points as a further validation of acquired PET images. SUV$_{liver}$ was not used as a reference in the final analysis.

Lesions were included in the final analysis if they were interpretable and measurable on standard-of-care imaging (24), if they were larger than 2 cm in diameter, and if they were identified on both PET session 1 and PET session 2, with both PET studies having been acquired at the same time after injection. In subjects with more than 5 visible lesions on PET session 1, the 5 lesions with the highest SUV$_{peak}$ were used. In all cases, the maximum number of selected lesions per organ was two.

Temporal Segmentation. In addition, list-mode data were temporally segmented after acquisition to characterize the efficacy of ^{18}F-fluciclatide as a function of administered activity (25). Injected activities of 25%, 50%, 75%, and 100% of the actual dose were simulated, and a masked image evaluation was performed to assess the fraction of the administered activity required to produce a diagnostic-quality image. Images were graded as excellent, moderate, poor, or nondiagnostic by 3

TABLE 1
Patient and Lesion Characteristics of Evaluable Tumors

Subject no.	Tumor type	No. in SoC	No. with PET uptake	No. RECIST-evaluable	FAS	SUV$_{peak}$ at 40 min
1	Breast	1	1	1	1	4.6
2	Breast	4	3	1	1	5.9
3	Breast	14	5	1	0	—
4	Breast	1	1	1	1	3.44
5	Breast	2	2	0	0	—
6	Breast	3	1	1	1	3.0
7	Breast	5	5	2	2	2.8, 10.1
8	Breast	3	1	1	1	3.6
9	Breast	5	2	2	2	4.8, 5.7
10	Breast	7	7	1	1	3.7
11	Breast	2	1	0	0	—
12	Breast	7	7	0	0	—
13	Breast	2	2	1	1	2.2
14	Colorectal carcinoma	6	1	0	0	—
15	Colorectal carcinoma	5	0	0	0	—
16	Colorectal carcinoma	3	3	2	2	2.8, 2.9
17	Colorectal carcinoma	6	4	2	2	2.3, 3.3
18	Colorectal carcinoma	4	2	2	2	1.4, 1.7
19	Colorectal carcinoma	1	1	1	0	—
20	Colorectal carcinoma	2	1	0	0	—
21	Colorectal carcinoma	4	4	0	0	—
22	Melanoma	7	4	2	2	6.6, 6.3
23	Melanoma	5	2	1	1	8.1
24	Ovarian	12	8	1	1	3.6
25	Ovarian	3	1	1	1	4.3
26	Cervical	5	1	0	0	—
27	Non–small cell lung cancer	8	2	2	2	3.5, 3.8
28	Malignant pheochromocytoma	13	8	5	5	5.3, 8.0, 10.1, 5.8, 4.4
29	Neuroendocrine	—	3	0	0	—
30	Neuroendocrine (gastrinoma)	9	2	2	1	2.5
31	Glioblastoma (grade IV)	1	1	1	1	3.2
32	Head and neck	6	5	0	0	—
33	Head and neck	3	1	1	1	9.7
34	Head and neck	11	5	3	3	4.2, 3.8, 2.7
35	Pancreatic	6	1	1	1	3.7
36	Pancreatic	7	1	1	1	4.9
37	Mesothelioma	3	1	1	1	5.3
38	Osteogenic sarcoma	1	1	0	0	—
39	Cancer of unknown primary	1	1	1	1	2.8
Total		188	102	42	39	

SoC = standard-of-care images; FAS = final analysis set.

independent interpreters. The Cohen κ statistic was used to measure agreement between ratings of overall image quality (*26*). Additionally, SUV$_{liver}$ and the coefficient of variation within the liver region of interest were measured across temporal fractions.

Determination of Sample Size and Statistical Analysis. The primary objective was to assess the reproducibility of ¹⁸F-fluciclatide. Previous single-center reproducibility studies with ¹⁸F-FDG reported a 10% variation in ¹⁸F-FDG uptake between repeated PET scans (*27*). Moreover,

FIGURE 1. ^{18}F-fluciclatide PET scan of 39-y-old man with diagnosis of melanoma. In rainbow-color-map image taken 65 min after injection, ^{18}F-fluciclatide uptake is seen within lung metastasis (arrow).

of less than 0.05 was considered significant, and statistical analysis was performed using R for Windows (Microsoft), version 3.0.1 (27).

RESULTS

Patient Population

Of the subgroup scheduled for immunochemical analysis, no biopsies were performed within the time window allowed by the protocol. The 4 subjects scanned within this group were therefore included in the main study group, to give a total of 39 patients (24 women and 15 men) recruited from 11 sites. The median age was 58.7 y (range, 29–86 y), and the most common tumor types were breast (21%) and colorectal (15%) (Table 1). The interval between PET sessions 1 and 2 ranged from 2 to 9 d (median, 5 d). The mean ($\pm$SD) start times of each acquisition during the first imaging session were 44 $\pm$ 11.8, 71 $\pm$ 11.9, and 98 $\pm$ 12.1 min. During the second imaging session, these were 44 $\pm$ 12.1, 71 $\pm$ 12.2, and 97 $\pm$ 12.4 min after injection. The mean administered activity was 327.2 MBq for PET session 1 (range, 262.9–374.8 MBq) and 326.6 MBq for PET session 2 (range, 271.8–363.8 MBq)

Tumor and Normal-Tissue Uptake of ^{18}F-Fluciclatide

Approximately half the lesions identified in the standard-of-care images exhibited measurable ^{18}F-fluciclatide uptake (Fig. 1). Mean SUV_{peak} at each time point in session 1 was 4.54 ($\pm$2.21) at 40 min, 4.63 ($\pm$2.34) at 65 min, and 4.39 ($\pm$2.25) at 90 min. The SUV data were not normally distributed ($P < 0.05$), but normality was restored by a logarithmic transform. Figure 2 illustrates the distribution of SUV_{peak} within tumor types. Regions of healthy liver tissue were identified in 20 subjects; mean SUV_{liver} was 3.94 $\pm$ 0.75 at 40 min after injection.

Reproducibility of ^{18}F-Fluciclatide SUV

Thirty-nine discrete lesions from 26 patients were evaluated for reproducibility of repeated measures of ^{18}F-fluciclatide retention; the other lesions did not fulfil the predefined criteria for lesion
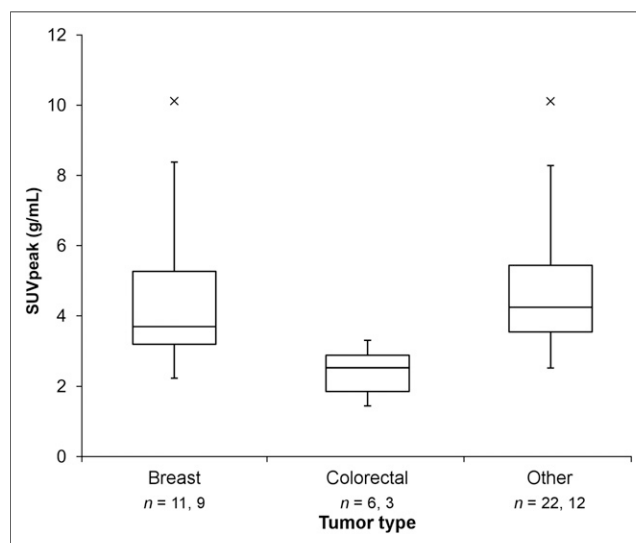
in evaluations of treatment response with ^{18}F-FDG, a 20%–30% decrease in tumor uptake suggests tumor response (28–30). Therefore, we assumed that, on the basis of ^{18}F-FDG data, intratumoral variation exceeding 15% was unlikely to be clinically useful (27). A sample size of 35 was chosen to give a 95% confidence interval of the mean relative difference with an SD of 0.15. A second group of 10 subjects, following the same protocol, was recruited to meet a secondary objective comparing SUV and immunohistochemical analysis of biopsied tissue. Concern that a biopsy would affect uptake meant these subjects were scheduled for a separate reproducibility analysis from the main group. Therefore, the total number of subjects to be enrolled was 45.

The reproducibility of SUV_{peak} was analyzed on a lesion-by-lesion basis. For reproducibility measures, the individual SUV_{peak} for each scanning visit was plotted for each acquisition time. High reproducibility was represented by all data being distributed along a line of unity. Correlation analysis and Wilcoxon signed-rank testing were used to assess reproducibility. The distribution of SUV for all lesions was assessed for normality using the Shapiro–Wilk test and the quantile–quantile plot and described as $SUV_{mean} \pm$ SD. The relative difference in uptake at each time point was defined as $2 \times (SUV_2 - SUV_1)/(SUV_1 + SUV_2)$, where SUV_1 is the SUV_{peak} in the first scanning session and SUV_2 is that in the second session. Box-and-whisker plots were generated to illustrate the distribution of the acquired data and mean relative differences. The 95% reference range from spontaneous fluctuations in SUV_{peak} was calculated as $1.96 \times$ SD of the relative difference between both PET scans. To provide further examination predicated on tumor type, additional analyses were performed for tumor types found in at least 3 subjects. Bland–Altman plots of the paired differences in SUVs were also examined. A P value

FIGURE 2. Box-and-whisker plot illustrating median and distribution of SUV_{peak} within lesions for each tumor subtype. Sample sizes (n) indicate both number of lesions measured and second number of subjects in each group. $\times$ = outliers.
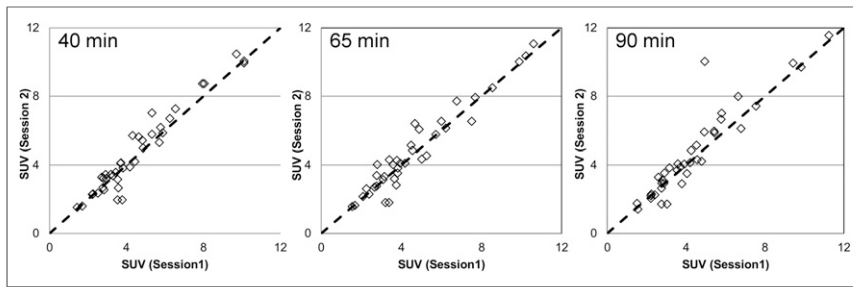
FIGURE 3. Test–retest scatterplots of SUV in session 2 (*y*-axis) against SUV in session 1 (*x*-axis) at 40, 65, and 90 min. Dotted line is line of unity.

selection (Table 1). Figure 3 shows plots of SUV_{peak} for the 2 PET sessions at the 3 acquisition times. No significant difference in SUV_{peak} between the 2 sessions was observed across the 3 acquisition points. Regression analysis of the line of unity indicated good test–retest correlation for the 3 acquisition times (Spearman r = 0.92, 0.94, and 0.94 at 40, 65, and 90 min, respectively). Figure 4 illustrates the variability of the relative difference. The mean relative differences were 0.01, 0.00, and 0.02 at 40, 65, and 90 min, respectively, with none being significantly different from zero. The SDs of the mean relative difference were 18%, 19%, and 20% for the 40-, 65-, and 90-min acquisition times, respectively. Intraclass correlation coefficients were, respectively, 0.96, 0.96, and 0.91 at the 3 acquisition times. These results indicate that SUV_{peak} obtained from ^{18}F-fluciclatide PET can be used repeatedly in serial scans. The 95% normal values for spontaneous fluctuations were 35%–39% (i.e., 1.96 × SD of relative difference).

The Bland–Altman plot of the differences between the 2 PET sessions at 40 min highlighting tumor types that occurred in more than 3 patients per group is shown in Figure 5. Overall, the mean difference in SUV_{peak} between the 2 sessions was 0.19, with 95% of the differences lying between the limits of agreement of 1.76 and −1.37. In breast cancer (11 lesions in 9 subjects), the mean relative difference was 0.00 ± 0.13, and in colorectal cancer it was 0.02 ± 0.08 (6 lesions in 3 subjects).

Temporal Segmentation

For uniformity, temporal segmentation was done using liver data. The κ statistics showed that the 2 interpreters' ratings of the 75%-activity images agreed substantially better with full-activity (100%) images than did 25%- or 50%-activity images, which were rated similarly in their degree of agreement with the full acquisition dataset (Fig. 6). Quantitatively, there was a reduction in SUV_{liver} with each successively smaller fraction (100%: 3.94 ± 0.36; 75%: 3.76 ± 0.40; 50%: 3.68 ± 0.47; 25%: 3.49 ± 0.59). The coefficient of variation for SUV_{liver} progressively increased as the fractional administered activity of ^{18}F-fluciclatide injection was reduced, indicating a progressively decreasing signal-to-noise ratio.

DISCUSSION

The primary aim of this study was to establish the serial reproducibility of ^{18}F-fluciclatide in a multicenter study to allow further investigation of this novel tracer as a biomarker of response to antiangiogenic and antiintegrin therapies. We have shown that ^{18}F-fluciclatide has good reproducibility in several tumor types at all 3 time points after administration, with mean relative SUV differences of 0%–2% between the 2 imaging sessions and an SD range of 18%–20% for the mean. This reproducibility is consistent with

reproducibility data obtained in large, multicenter studies assessing ^{18}F-FDG and is acceptable for evaluation of tumor response to therapy (*27*).

Despite the widespread use of antiangiogenic drugs in the therapeutic setting, there are no validated biomarkers of response to therapy. Measurement of microvessel density by immunohistochemistry is the gold standard by which tumor angiogenesis is assessed. However, serial tumor biopsies are generally not acceptable in the clinical setting, and heterogeneity of microvessel density within the tumor limits the utility of this procedure further (*31*). A noninvasive method of assessing changes to tumor vasculature in response to treatment is therefore needed. There is expanding literature on the notion that tumor uptake of radiolabeled RGD peptides can reflect the angiogenesis phenotype. For example, tumor uptake of the RGD peptide ^{18}F-galacto-RGD correlates with microvessel density (*32,33*). Moreover, Battle et al. demonstrated a serial reduction in ^{18}F-fluciclatide uptake in tumors after treatment with the antiangiogenic agent sunitinib; a corresponding reduction in microvessel density was also observed (*34*). These findings are in keeping with the high affinity of RGD sequences for integrins expressed on tumor endothelial cells as reported by Pasqualini et al. (*35*). The ability of ^{18}F-fluciclatide and other RGD probes to detect angiogenesis phenotype may be less dependent on tumor cell expression of the receptor. Melanoma, for example, has a higher expression of $\alpha_v\beta_3$ integrin in tumor cells than in the associated vasculature. However, work by our group, considering the uptake of ^{68}Ga-DOTA-[c(RGDfK)]$_2$ in melanoma and breast cancer models with varying $\alpha_v\beta_3$ expression, indicates that although the binding kinetics of RGD probes are influenced by $\alpha_v\beta_3$ expression on cells in vivo, the vessel fraction of $\alpha_v\beta_3$ integrin contributes maximally to the uptake of RGD probe, supporting its role as a biomarker of angiogenesis (*36*).

Several other tracers based on the cyclic RGD structure have been developed, with ^{18}F-galacto-RGD being the only other probe
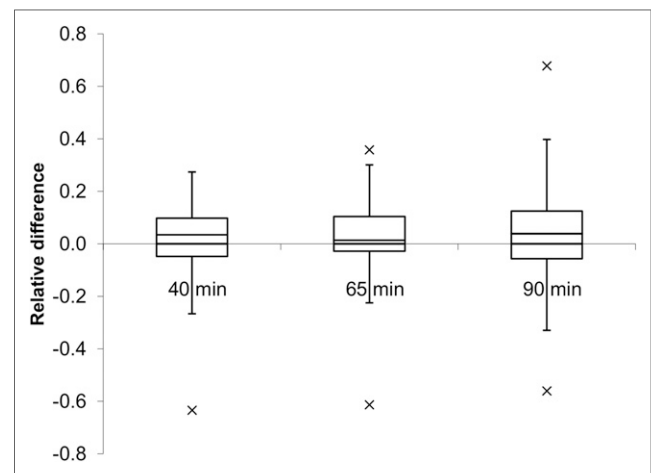

FIGURE 4. Box plot illustrating relative difference in SUV_{peak} at 40, 65, and 90 min after injection. Plot shows median relative difference. × = outliers.
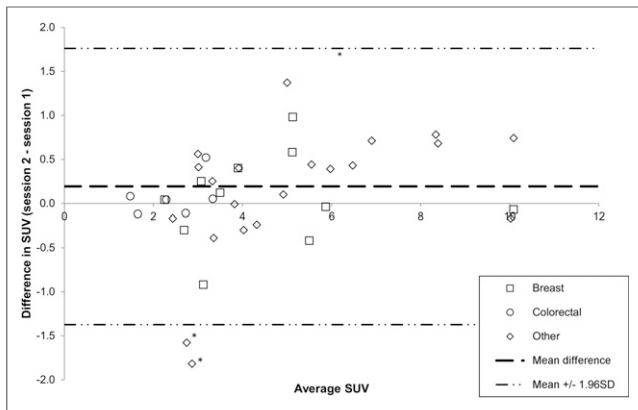
FIGURE 5. Bland–Altman plot of difference in SUV at 40 min against SUV$_{mean}$. Outliers are from subject with NSCLC. *Lung lesions.

to have undergone clinical studies, which showed SUV to correlate with $\alpha_v\beta_3$ expression in tumors (*32*). Other imaging modalities consider functional parameters such as blood flow, vessel permeability, and blood volume as surrogates of angiogenesis. Clinically, dynamic contrast-enhanced CT and MRI are widely used (*37*). However, clinical trials have demonstrated marked heterogeneity in the results obtained, with no correlation with response to antiangiogenic therapies being observed (*38*). Therefore, probes that directly image $\alpha_v\beta_3$ on tumor vasculature hold promise.

Knowledge of the precision of repeated imaging parameters is a prerequisite for serial response measurements and, therefore, response to treatment. Our study found no significant change in SUV$_{peak}$ between the 2 scans; the 95% reference range of spontaneous fluctuations was 35%–39%. Thus, with the current protocol, a reduction in SUV$_{peak}$ of at least 39% within any given lesion can be classified as an ^{18}F-fluciclatide response. A similar level of reproducibility has been reported for ^{18}F-FDG in a diverse range of tumor types and for ^{18}F-fluorothymidine in breast cancer (*27,39*). Furthermore, our findings agree with those of Doot et al., who suggested that an SD of 20% in relative SUV change is typical of a multicenter trial with good calibration (*23*).

Not all tumors were visualized on ^{18}F-fluciclatide PET scans compared with standard-of-care imaging. Because ^{18}F-fluciclatide binds with high affinity to $\alpha_v\beta_3/\alpha_v\beta_5$ integrin, uptake of the tracer may be linked to differential expression of $\alpha_v\beta_3/\alpha_v\beta_5$ integrin within tumors. Beer et al. reported an 80% uptake of ^{18}F-galacto-RGD

in patients with malignancy and reported a correlation between SUV and expression of $\alpha_v\beta_3$ both within the tumor and within its associated microvasculature (*17*). Variability in uptake of both ^{18}F-fluciclatide and ^{18}F-galacto-RGD may reflect differential growth of tumors, with the expression of $\alpha_v\beta_3$ playing an important role during the initial phases of tumor growth, whereas an alternative angiogenic signaling mechanism may be more involved in metastases. Furthermore, tumor size may affect tracer uptake, with large tumors generally demonstrating areas of neoangiogenesis around the tumor periphery and the central area being relatively hypoxic, containing areas of necrosis.

In individual tumor types, Bland–Altman plotting indicated poor reproducibility for lung lesions and a case of renal cell cancer. Low reproducibility may be attributed to physiologic motion, particularly in patients with pleural lesions. Application of respiratory motion techniques may improve reliability in future studies. Pelvic lesions also showed reduced reproducibility, because physiologic uptake of ^{18}F-fluciclatide within the bladder made their assessment difficult, a common limitation with ^{18}F-FDG. Urinary excretion may have also contributed to the adverse reproducibility of the renal tumor. Although most lesions observed on standard-of-care imaging were observed on PET imaging, several lesions were not observed. Some lesions were based within the liver, where physiologic accumulation of ^{18}F-fluciclatide occurs as a result of both metabolism and the dense vasculature of the liver, hampering visualization of hepatic tumors. Therefore, the clinical application of ^{18}F-fluciclatide may be limited in those patients with predominantly pelvic and hepatic disease. However, a key issue directly affecting uptake of ^{18}F-fluciclatide will be the expression level of $\alpha_v\beta_3/\alpha_v\beta_5$ integrin within the tumor and associated vasculature. Future studies would benefit from correlation of ^{18}F-fluciclatide uptake characteristics with $\alpha_v\beta_3/\alpha_v\beta_5$ integrin expression within the tumor.

Temporal segmentation visual analysis did not identify large differences in image quality between 25% and 50% data despite the decreasing signal-to-noise ratio observed in the quantitative study of liver SUV. The mean SUV$_{peak}$ decreased with increasing frame times. This is a slightly unusual result because increased image noise (e.g., in short dynamic image frames with low counts) usually results in a positive bias in SUV due to the nonnegativity constraint of ordered-subset expectation maximization reconstruction. However, because the SUV reported is far from zero, this effect should be small. One possible explanation is that the corrections (e.g., dead time and scatter) applied to the emission data are always based on the full acquisition and errors are introduced as the temporal segment is reduced.
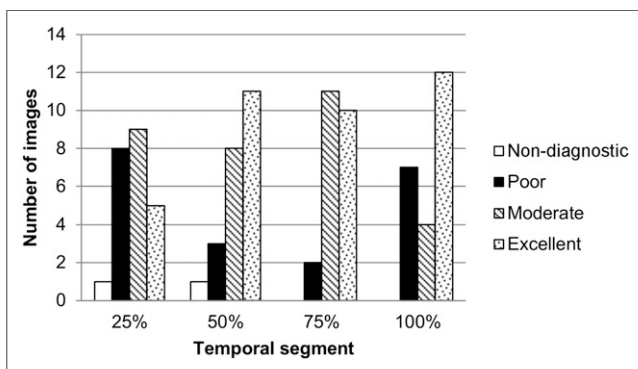
CONCLUSION

We have shown in a multicenter study that ^{18}F-fluciclatide PET imaging can be conducted with high reproducibility in several tumor types including breast and colorectal cancer and warrants further investigation as a response biomarker to antiangiogenic therapies.

DISCLOSURE

FIGURE 6. Assessment of image quality of temporally segmented image data.

research funded by GE Healthcare. No other potential conflict of interest relevant to this article was reported.

REFERENCES

1. Folkman J. Angiogenesis in cancer, vascular, rheumatoid and other disease. *Nat Med.* 1995;1:27–31.
2. Aghajanian C, Blank SV, Goff BA, et al. OCEANS: a randomized, double-blind, placebo-controlled phase III trial of chemotherapy with or without bevacizumab in patients with platinum-sensitive recurrent epithelial ovarian, primary peritoneal, or fallopian tube cancer. *J Clin Oncol.* 2012;30:2039–2045.
3. Cassidy J, Clarke S, Diaz-Rubio E, et al. Randomized phase III study of capecitabine plus oxaliplatin compared with fluorouracil/folinic acid plus oxaliplatin as first-line therapy for metastatic colorectal cancer. *J Clin Oncol.* 2008;26: 2006–2012.
4. Hurwitz H, Fehrenbacher L, Novotny W, et al. Bevacizumab plus irinotecan, fluorouracil, and leucovorin for metastatic colorectal cancer. *N Engl J Med.* 2004; 350:2335–2342.
5. Saltz LB, Clarke S, Diaz-Rubio E, et al. Bevacizumab in combination with oxaliplatin-based chemotherapy as first-line therapy in metastatic colorectal cancer: a randomized phase III study. *J Clin Oncol.* 2008;26:2013–209.
6. Motzer RJ, Hutson TE, Tomczak P, et al. Sunitinib versus interferon alfa in metastatic renal-cell carcinoma. *N Engl J Med.* 2007;356:115–124.
7. Perren TJ, Swart AM, Pfisterer J, et al. A phase 3 trial of bevacizumab in ovarian cancer. *N Engl J Med.* 2011;365:2484–2496.
8. Llovet JM, Ricci S, Mazzaferro V, et al. Sorafenib in advanced hepatocellular carcinoma. *N Engl J Med.* 2008;359:378–390.
9. Brooks PC, Clark RA, Cheresh DA. Requirement of vascular integrin alpha v beta 3 for angiogenesis. *Science.* 1994;264:569–571.
10. Giancotti FG, Ruoslahti E. Integrin signaling. *Science.* 1999;285:1028–1032.
11. Friedlander M, Brooks PC, Shaffer RW, Kincaid CM, Varner JA, Cheresh DA. Definition of two angiogenic pathways by distinct alpha v integrins. *Science.* 1995;270:1500–1502.
12. Plow EF, Haas TA, Zhang L, Loftus J, Smith JW. Ligand binding to integrins. *J Biol Chem.* 2000;275:21785–21788.
13. Lang L, Li W, Guo N, et al. Comparison study of [18F]FAl-NOTA-PRGD2, [18F]FPPRGD2, and [68Ga]Ga-NOTA-PRGD2 for PET imaging of U87MG tumors in mice. *Bioconjug Chem.* 2011;22:2415–2422.
14. Kenny LM, Coombes RC, Oulie I, et al. Phase I trial of the positron-emitting Arg-Gly-Asp (RGD) peptide radioligand 18F-AH111585 in breast cancer patients. *J Nucl Med.* 2008;49:879–886.
15. Janssen ML, Oyen WJ, Dijkgraaf I, et al. Tumor targeting with radiolabeled alpha$_v$beta$_3$ integrin binding peptides in a nude mouse model. *Cancer Res.* 2002;62:6146–6151.
16. Wu Z, Li ZB, Chen K, et al. microPET of tumor integrin alphavbeta3 expression using 18F-labeled PEGylated tetrameric RGD peptide (18F-FPRGD4). *J Nucl Med.* 2007;48:1536–1544.
17. Beer AJ, Grosu AL, Carlsen J, et al. [18F]galacto-RGD positron emission tomography for imaging of alphavbeta3 expression on the neovasculature in patients with squamous cell carcinoma of the head and neck. *Clin Cancer Res.* 2007;13: 6610–6616.
18. Indrevoll B, Kindberg GM, Solbakken M, et al. NC-100717: a versatile RGD peptide scaffold for angiogenesis imaging. *Bioorg Med Chem Lett.* 2006;16: 6190–6193.
19. McParland BJ, Miller MP, Spinks TJ, et al. The biodistribution and radiation dosimetry of the Arg-Gly-Asp peptide 18F-AH111585 in healthy volunteers. *J Nucl Med.* 2008;49:1664–1667.
20. Wahl RL, Jacene H, Kasamon Y, Lodge MA. From RECIST to PERCIST: evolving considerations for PET response criteria in solid tumors. *J Nucl Med.* 2009;50(suppl 1):122S–150S.
21. Frank R, Group F-PCW. Quantitative Imaging Biomarkers Alliance FDG-PET/CT Working Group report: molecular imaging and biology. *Mol Imaging Biol.* 2008;10:305.
22. Bland JM, Altman DG. A note on the use of the intraclass correlation coefficient in the evaluation of agreement between two methods of measurement. *Comput Biol Med.* 1990;20:337–340.
23. Doot RK, Kurland BF, Kinahan PE, Mankoff DA. Design considerations for using PET as a response measure in single site and multicenter clinical trials. *Acad Radiol.* 2012;19:184–190.
24. Eisenhauer EA, Therasse P, Bogaerts J, et al. New response evaluation criteria in solid tumours: revised RECIST guideline (version 1.1). *Eur J Cancer.* 2009;45: 228–247.
25. Bailey DL, Kalemis A. Externally triggered gating of nuclear medicine acquisitions: a useful method for partitioning data. *Phys Med Biol.* 2005;50:N55–N62.
26. Sim J, Wright CC. The kappa statistic in reliability studies: use, interpretation, and sample size requirements. *Phys Ther.* 2005;85:257–268.
27. Weber WA, Ziegler SI, Thodtmann R, Hanauske AR, Schwaiger M. Reproducibility of metabolic measurements in malignant tumors using FDG PET. *J Nucl Med.* 1999;40:1771–1777.
28. Avril N, Sassen S, Schmalfeldt B, et al. Prediction of response to neoadjuvant chemotherapy by sequential F-18-fluorodeoxyglucose positron emission tomography in patients with advanced-stage ovarian cancer. *J Clin Oncol.* 2005;23:7445–7453.
29. Weber WA, Petersen V, Schmidt B, et al. Positron emission tomography in non-small-cell lung cancer: prediction of response to chemotherapy by quantitative assessment of glucose use. *J Clin Oncol.* 2003;21:2651–2657.
30. Minn H, Zasadny KR, Quint LE, Wahl RL. Lung cancer: reproducibility of quantitative measurements for evaluating 2-[F-18]-fluoro-2-deoxy-D-glucose uptake at PET. *Radiology.* 1995;196:167–173.
31. Hlatky L, Hahnfeldt P, Folkman J. Clinical application of antiangiogenic therapy: microvessel density, what it does and doesn't tell us. *J Natl Cancer Inst.* 2002;94: 883–893.
32. Beer AJ, Haubner R, Sarbia M, et al. Positron emission tomography using [18F]galacto-RGD identifies the level of integrin alpha$_v$beta3 expression in man. *Clin Cancer Res.* 2006;12:3942–3949.
33. Haubner R, Weber WA, Beer AJ, et al. Noninvasive visualization of the activated alphavbeta3 integrin in cancer patients by positron emission tomography and [18F]galacto-RGD. *PLoS Med.* 2005;2:e70.
34. Battle MR, Goggi JL, Allen L, Barnett J, Morrison MS. Monitoring tumor response to antiangiogenic sunitinib therapy with 18F-fluciclatide, an 18F-labeled alphaVbeta3-integrin and alphaV beta5-integrin imaging agent. *J Nucl Med.* 2011; 52:424–430.
35. Pasqualini R, Koivunen E, Ruoslahti E. Alpha v integrins as receptors for tumor targeting by circulating ligands. *Nat Biotechnol.* 1997;15:542–546.
36. Alam IS, Witney TH, Tomasi G, et al. Radiolabeled RGD tracer kinetics annotates differential alphavbeta 3 integrin expression linked to cell intrinsic and vessel expression. *Mol Imaging Biol.* 2014;16:558–566.
37. Dobrucki LW, de Muinck ED, Lindner JR, Sinusas AJ. Approaches to multimodality imaging of angiogenesis. *J Nucl Med.* April 15, 2010 [Epub ahead of print].
38. Zweifel M, Padhani AR. Perfusion MRI in the early clinical development of antivascular drugs: decorations or decision making tools? *Eur J Nucl Med Mol Imaging.* 2010;37(suppl 1):S164–S182.
39. Kenny L, Coombes RC, Vigushin DM, Al-Nahhas A, Shousha S, Aboagye EO. Imaging early changes in proliferation at 1 week post chemotherapy: a pilot study in breast cancer patients with 3′-deoxy-3′-[18F]fluorothymidine positron emission tomography. *Eur J Nucl Med Mol Imaging.* 2007;34:1339–1347.